AUT Journal of Mechanical Engineering

AUT J. Mech. Eng., 1(2) (2017) 219-232
DOI: 10.22060/mej.2017.12863.5455

Computational Investigation of Unsteady Compressible Flow over a Fixed Delta Wing Using Detached Eddy Simulation

H. Ansarian*, M. Hadidoolabi

Malek Ashtar University of Technology, Tehran, Iran

ABSTRACT: Unsteady compressible flows over a stationary 60-degree swept delta wing with a sharp leading edge were computationally simulated at different Mach numbers and moderate angles of the attack. An unstructured grid, Spalart-Allmaras Detached Eddy Simulation turbulence model, and a dual-time implicit time integration were used. Vortical flow structures associated with various free-stream conditions are displayed and their variations versus time are studied. Variations of flow field parameters, such as u velocity component and pressure coefficient with the flow time are demonstrated at several point probes in the flow field. A Power Spectral Density frequency analysis is performed for such unsteady behaviours to identify the dominant frequencies which exist in each flow condition. The frequency analyses show that low frequencies associated with vortex breakdown oscillation are the most dominant frequencies in all cases where vortex breakdown occurs. Dominant frequencies associated with helical mode instability are also present at the probes downstream of breakdown. Dominant frequencies related to the shear layer instabilities were observed for the low subsonic regime.

Review History:

Received: 7 May 2017
Revised: 28 June 2017
Accepted: 16 July 2017
Available Online: 21 October 2017

Keywords:

Delta wing
Unsteady flow
DES turbulence model
Frequency analysis

1- Introduction

It is well known that the flow over a delta wing is characterized by the vortical structures, mainly the leading edge vortices [1-3]. As the angle of the attack increases enough, the adverse pressure gradient which exists in the flow causes vortex breakdown to occur over the wing. This flow is found to be highly unsteady and may have a large impact on the wing behaviour. For aeroelastic and flight mechanics behaviours, such as buffeting of existing configurations, it is clear that understanding the behaviour of unsteady loading is crucial to allow the alleviation of all possible structural responses. This is particularly important for complex fighter configurations such as the Euro Fighter and F16XL and is compounded by the emergence of the new UCAV and UAV technologies, which are tending toward planforms where time-dependent vortical flows play an impressive role. Therefore, the need for a more complete and accurate understanding of the unsteady nature of such vortical structures is becoming increasingly important.

A great deal of research has been focused on the behaviour of delta wing flows which is summarized in the reviews by Gursul [1,2] and by Nelson and Pelletier [3]. From these studies, it is evident that the unsteady behaviour of vortical flows is complicated since a large number of flow phenomena exist and interact over the wing and its downstream. These flow phenomena include the vortex wandering, shear layer instabilities, helical mode instability of vortex breakdown and vortex breakdown oscillations. By reviewing the related literature available, Schiavetta et al. [4] reported that some patterns emerge that relate these flow features to the order and size of the non-dimensional frequencies. A summary of these unsteady flow features with their corresponding non-dimensional frequency ranges is shown in Table 1. Strouhal number which is non-dimensional frequency is defined as $St=fc/U_{\infty}$.

Corresponding author, E-mail: ansarianh@mut.ac.ir

Table 1. Frequencies corresponding to important unsteady phenomena of vortical flows

Phenomenon	Strouhal number
Helical mode instability	1-2
Shear layer instabilities	8-10 and higher
Vortex shedding- T.E	~8
Vortex shedding- high	0.2-0.5
Vortex breakdown oscillation	0.01-0.08

Of course, there are other dominant frequencies observed, which are not clearly attributed to a particular phenomenon. These are St=2.5-4, 5-6 and the higher frequencies ~ 20. It is possible that they also correspond to the phenomena mentioned above, however further studies are required. It is important to note that there may be more than one dominant frequency associated with a specific phenomenon, because of the complexity of the flow unsteady nature. For example, the shear layer instability will have at least two associated frequencies. This is because of the fact that the shear layer rolls up into discrete sub-vortices, which will demonstrate a frequency of rotation and also that these structures move around the vortex core. Although it seems difficult to separate these frequencies within a single solution, it may be helpful to express the distribution of data and assign the dominant frequencies to the particular flow features.

For the further understanding of the unsteady behaviour of the flow, it is useful to divide these phenomena into two categories, those which occur upstream of breakdown location and those which occur downstream, as shown in Fig. 1. Classifying the unsteady features in this way

allows to clarify which features will dominate, depending on the position of vortex breakdown on the wing. For a breakdown close to the wing apex, it is likely that the helical mode instability would dominate the flow. However as the breakdown moves downstream, it is likely that the shear layer attachment and shear layer instabilities may dominate the flow frequency content. This will be important when looking at the flow overall and considering the frequency content of the results, especially when considering the unsteady loading on the wing.

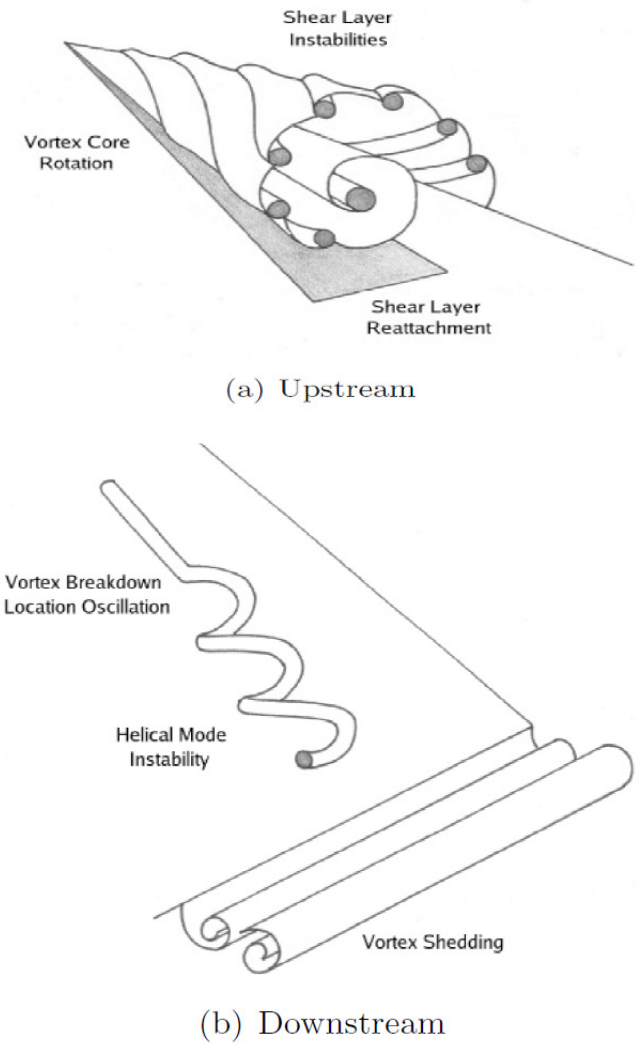

Fig. 1. Schematic diagrams showing flow topology upstream and downstream of vortex breakdown [4]

Simulating this complex flow and predicting its features accurately is a challenge for numerical methods. In recent years, the development of CFD algorithms with more complex turbulence modelling and the treatments being utilized have improved the capabilities of numerical solvers. Detached Eddy Simulation (DES) is one such method, which is a hybrid URANS/LES turbulence treatment, proposed initially by Spalart et al. [5]. The fine grid resolution in the boundary layer region which is needed for high Reynolds number LES calculations is reduced by DES method. It works by applying URANS to the boundary layer region and LES to the majority of the flow domain. This means that the majority of turbulence inside the flow domain is simulated, with only the small-scale eddies within the boundary layer being modelled. Using this treatment, many of the higher turbulent frequencies in the flow can be captured, which leads to a better ability to predict more complex flow behaviours accurately. This has been proved by DES calculations performed on various delta wing geometries (Mitchell et al., [6], and Morton, [7]).

Most of the studies performed for unsteady aspects of the flow over a fixed delta wing have dealt with incompressible or very low Mach number flows. Experimental and numerical studies which are previously performed for supersonic flows over delta wings report only time-averaged flow patterns or aerodynamic characteristics [8-10]. The objective of the present work is to extend the study of the unsteady behaviour of delta wing flows to the compressible regimes, especially the supersonic regime, with the aid of numerical simulations. To do this, the unsteady turbulent flow field over a fixed delta wing at moderate angles of attack and different sound regimes was solved. Vortical flow structures associated with various free-stream conditions are simulated and their variations with time are studied. Variations of flow field parameters, such as velocity component and pressure coefficient with the flow time are demonstrated. A frequency analysis is performed for such unsteady behaviours to identify the dominant frequencies which exist in each flow condition. The effects of Mach number and angle of attack on the dominant frequencies are studied.

2- Methodologies

2- 1- Model Geometry and Grid

The model geometry is illustrated in Fig. 2. As shown in the figure, the analyzed delta wing has a leading edge sweep angle of 60°. The upper surface is flat and the leading edge is sharp (10° angle between the upper and lower surfaces) to minimize the effect of the leading edge shape on the flow field. Maximum wing thickness ratio is 0.03 based on the root chord length. The flow field is considered to be symmetric on the centre line of the wing. Therefore, only half of the wing is covered by the computational domain.

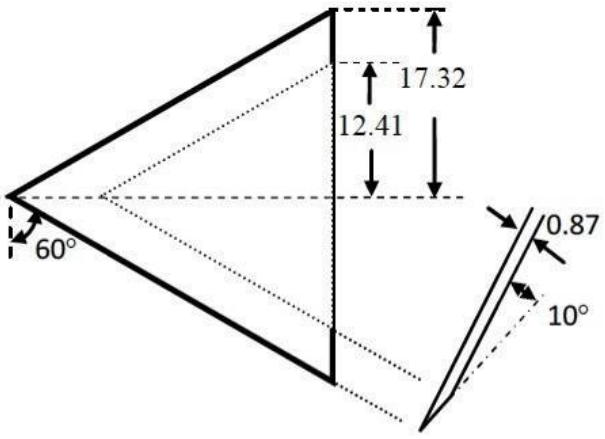

Fig. 2. Model Geometry

All simulations were computed on unstructured meshes with triangle-based prisms in the boundary layer and tetrahedral elsewhere (Fig. 3). The grid has approximately 1.3×10^7 cells and has been obtained from extensive simulations for grid independence study. Since the objective of this study is to

simulate the flow pattern accurately, grid independence study was performed by checking the convergence of the numeric values of flow field variables in several flow field points, for several steady flow conditions. An example is shown in Fig. 4 for the time-averaged dimensionless axial and tangential velocities at an arbitrary point near the vortex core, for the flow with Mach number of 1.2 and angle of attack of 30º. The convergence of aerodynamic coefficients could be attained by much coarser grids. The grid has a first wall spacing of $y^+\approx1$. This value is appropriate for the turbulence model used. A spatial zone of very fine mesh was created around the wing which contains the vortical flow region. This helps to improve the grid quality for the application of DES and capturing the vortices well. The upper and lower surfaces of the wing were specified as a solid wall with no-slip boundary conditions and no heat transfer. The symmetry boundary condition was applied to the symmetry plane. The remaining domain is a hemisphere with diagonal of 15 root chord length and was specified as the pressure farfield. Free stream parameters such as Mach number and angle of attack are set at the pressure farfield boundary.

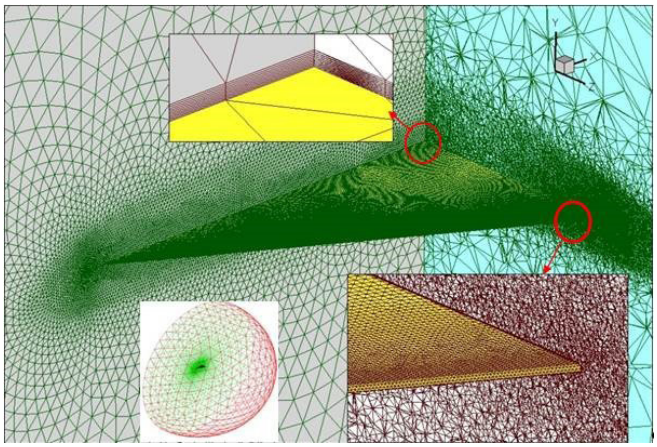

Fig. 3. Computational grid

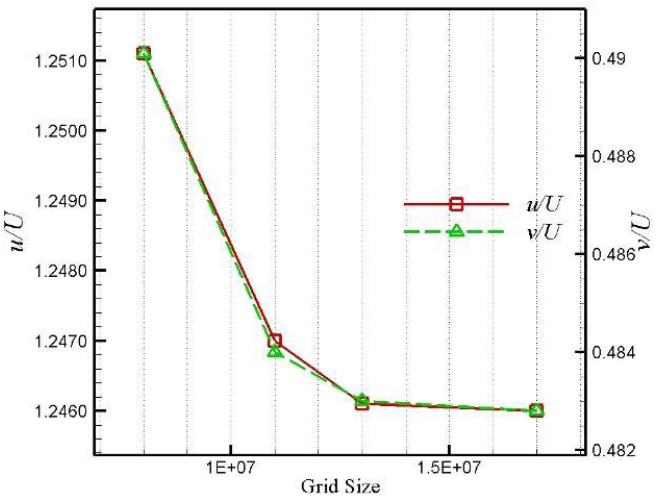

Fig. 4. Time-averaged axial and tangential velocity components in an arbitrary point for various grid sizes

2- 2- Computational Methods

Three-dimensional unsteady compressible Navier-Stokes equations are solved as the governing equations. Numerical fluxes for the convective terms are computed using the Roe's scheme and the upwind MUSCL algorithm is applied to extend the spatial accuracy to 2nd order based on the primitive variables. The viscous fluxes are computed using the 2nd order central differencing. The flow field is assumed to be fully turbulent and the SA-DES model is used. An implicit dual-time algorithm is applied for the unsteady time integration. A parallel processing was applied in order to accelerate the solution. Density was calculated by ideal gas law and viscosity by Sutherland's law. A valid CFD code was available for the authors which had capabilities mentioned above (Hadidoolabi and Ansarian [11, 12]).

The Spalart-Allmaras (SA) one equation model solves a single PDE for a working variable which is related to the turbulent viscosity. The PDE is derived by "using empiricism and arguments of dimensional analysis, Galilean invariance and selected dependence on the molecular viscosity" (Spalart and Allmaras [13]). The SA model has a low computational cost and is known for giving acceptable results for aerodynamic applications, boundary layers subjected to adverse pressure gradients, supersonic flows, and unstructured meshes. The model contains a wall destruction term which reduces the turbulent viscosity in the laminar sublayer. The differential equation has the form,

$$\frac{\partial\tilde{\nu}}{\partial t}+\frac{\partial\left(\tilde{\nu}u_j\right)}{\partial x_j}=c_{b1}\tilde{S}\tilde{\nu}-c_{w1}f_w\left(\frac{\tilde{\nu}}{d}\right)^2 +\frac{1}{\sigma}\frac{\partial}{\partial x_k}\left[\left(\nu+\tilde{\nu}\right)\frac{\partial\tilde{\nu}}{\partial x_k}\right]+\frac{c_{b2}}{\sigma}\frac{\partial\tilde{\nu}}{\partial x_k}\frac{\partial\tilde{\nu}}{\partial x_k} \quad (1)$$

The turbulent kinematic viscosity is calculated from

$$\nu_T=\frac{\mu_T}{\rho}=\tilde{\nu}f_{v1} \quad (2)$$

where $f_{v1}=\frac{\chi^3}{\chi^3+c_{v1}^3}$, $\chi=\frac{\tilde{\nu}}{\nu}$, and S is the vorticity magnitude given by

$$S=|\omega|=\left|\nabla\times\left(u\hat{i}+v\hat{j}+w\hat{k}\right)\right| \quad (3)$$

and the modified vorticity is

$$\tilde{S}=S+\frac{\tilde{\nu}}{\kappa^2d^2}f_{v2},\quad f_{v2}=1-\frac{\chi}{1+\chi f_{v1}} \quad (4)$$

where d is the distance to the closest wall. The wall destruction function f_w is

$$f_w=g\left[\frac{1+c_{w3}^6}{c_{w3}^6}\right]^{1/6} \quad (5)$$

with $g=r+c_{w2}\left(r^6-r\right)$ and $r=\frac{\tilde{\nu}}{\tilde{S}\kappa^2d^2}$.

The turbulent viscosity is obtained from the turbulent kinematic viscosity by $\mu_T=\rho\nu_T$. Table 2 gives the model coefficients.

The Detached Eddy Simulation method was introduced by Spalart et al. [5] and was originally based on the Spalart-Allmaras one equation RANS model. The wall destruction

Table 2. Model coefficients for the Spalart-Allmaras turbulence model, where $c_{w1}=c_{b1}/\kappa^2+(1+c_{b2})/\sigma$

c_{t1}	c_{t2}	c_{v1}	c_{w1}	c_{w2}	c_{w3}
0.1355	0.622	7.1	3.239	0.3	2.0
c_{t1}	c_{t2}	c_{t3}	c_{t4}	σ	κ
1.0	2.0	1.1	2.0	2/3	0.41

term in Eq. (1) is proportional to $(\tilde{\nu}/d)^2$. When this term is balanced with the production term, the eddy viscosity becomes proportional to $\hat{S}d^2$, where $\hat{S}$ is the local strain rate. In the Smagorinsky LES model, the sub-grid scale (SGS) turbulent viscosity is proportional to the local strain rate and the grid spacing: $\nu_{SGS}\propto\hat{S}\Delta^2$, where $\Delta=\max(\Delta x,\Delta y,\Delta z)$. In the wall destruction term, if d is replaced with Δ, the Spalart-Allmaras model will act as the Smagorinsky LES model. To exhibit both LES and URANS behaviours, d in the Spalart-Allmaras model is replaced by the following parameter:

$$\tilde{d}=\min\left(d,C_{DES}\Delta\right) \quad (6)$$

When $d>>\Delta$ the model acts in the Smagorinsky LES mode and when $d<<\Delta$, the model acts in the URANS mode. Thus, the model switches into LES mode when the grid is locally refined.

Forsythe et al. [14] implemented the DES in an unstructured grid method and showed that the DES constant should be C_{DES}=0.65, when the grid spacing, Δ, was defined as the longest distance between the cell centre and all of its neighboring cell centers. It was consistent with the structured grid implementation of Spalart et al. [5].

2- 3- Flow Conditions

To investigate the effects of Mach number and angle of attack on the dominant frequencies which occur in the unsteady flow, six cases for flow conditions were chosen, as shown in Table 3. The time step used to update the solution was 10^{-6} seconds for all conditions. To assure convergence, a number of 40 sub-iterations were run for each time step.

Table 3. Flow Conditions

M_∞	α
0.4	20°
0.8	20°
0.8	24°
1.2	30°
2	30°
2	44°

3- Results and Discussion

3- 1- Unsteady Behaviour of Flow Structure

Different possible flow structures over a stationary delta wing in compressible regimes were studied experimentally by several researchers e.g. Miller and Wood [8], Seshadry and Narayan [9], and Brodetsky et al. [10]. The present authors [11, 12] simulated these flow structures over a stationary delta wing by time-averaged numerical simulations and also studied their variations during a pitching motion. In this section, it is discussed how a DES solution of flow over a stationary delta wing varies with the time.

Figs. 5 to 7 show the flow structure variation over the wing for three different flow conditions. Each figure contains the contours of the flow pattern in three randomly chosen instants of time. On the left snapshots are shown the local Mach number contour map and total pressure contour lines in a crossflow plane at 30% chordwise station. In the right snapshots are shown the local Mach number distribution in a plane crossing the primary vortex axis, and also the crossflow plane at 60% chordwise station. For M_∞=0.4, α=20° (Fig. 5), the type of flow field is classical vortex characterized by the primary and secondary vortices with no shock waves. No change happens in the type of flow pattern during this time interval, although some changes in Mach number distribution are observed. The flow over the leeside of the wing experiences breakdown before reaching the 60% chordwise station. Vortex breakdown does not reach the 30% chordwise station. Obviously, the flow structure after breakdown varies with the time in a random manner.

For M_∞=0.8, α=24° (Fig. 6), the type of the flow field is again classical vortex. However, some differences exist between this case and the previous one. The breakdown in the flow is observed over the lee-surface of the wing and its structure and position oscillate with time. Flow patterns at the 30% chordwise station are totally different at various time instants since the breakdown location oscillates near this station. At the first time instant, the breakdown is seen in the second separation region. At the second time instant, the breakdown is seen in the primary vortex region. Both primary and secondary vortices exist in the third instant of time since the breakdown location has moved downstream. As can be seen in this figure, a crossflow shock wave arises below the primary vortex core. Adverse pressure gradient due to this shock wave enhances the secondary flow separation.

By increasing Mach number and angle of attack, the flow above the pair of primary vortices and the vortex sheet becomes conically supersonic (the projection of the velocity vector onto a crossflow plane is greater than the velocity of sound). The axial rotation of two conically supersonic flows directed from the leading edges to the plane of the central symmetry toward each other gives rise to the spanwise flow acceleration and creates the internal shock waves above the pair of primary vortices. This structure is called vortex with the shock pattern. Further increase in the angle of attack leads to a greater strength of the shock wave above the vortex; it extends upward to a greater distance from the vortex core. This shock decelerates the flow toward the wing root and changes the flow direction. For M_∞=2, α=44° (Fig. 7), the type of the flow field is vortex with the shock. Although vortex breakdown over a delta wing in supersonic regimes has not been addressed in the previous studies, it may occur if the angle of attack is large enough. Similar to Fig. 5, the breakdown position oscillates near the 30% chordwise station in Fig. 7. At the first time instant, the breakdown is seen in both primary vortex and secondary separation regions. At the second time instant, the breakdown is seen in the secondary separation region and some parts of the shear layer. In the third time instant, only the secondary separation region has experienced a breakdown. A crossflow shock wave is seen below the primary vortex core in this time instant. In M_∞=2, α=44° condition, a horizontal shock wave appears between the pair of primary vortices. This shock wave is located approximately at an unchanged stand-off distance from the wing, but its size and strength are affected by the surrounding flow features.

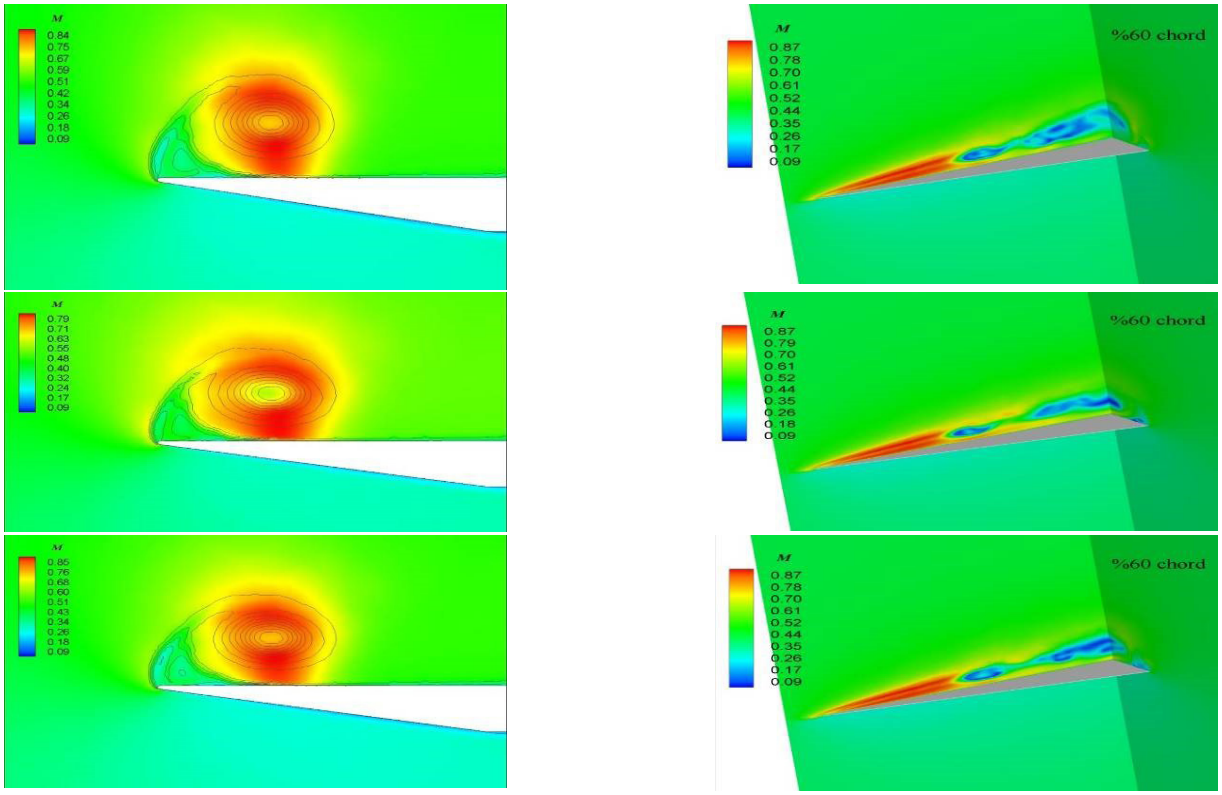

Fig. 5. Variation of flow structure with M_∞=0.4, α=20° around the wing in three random instants of time: at 30% chordwise station (left) and 60% chordwise station and a plane crossing the vortex axis (right)

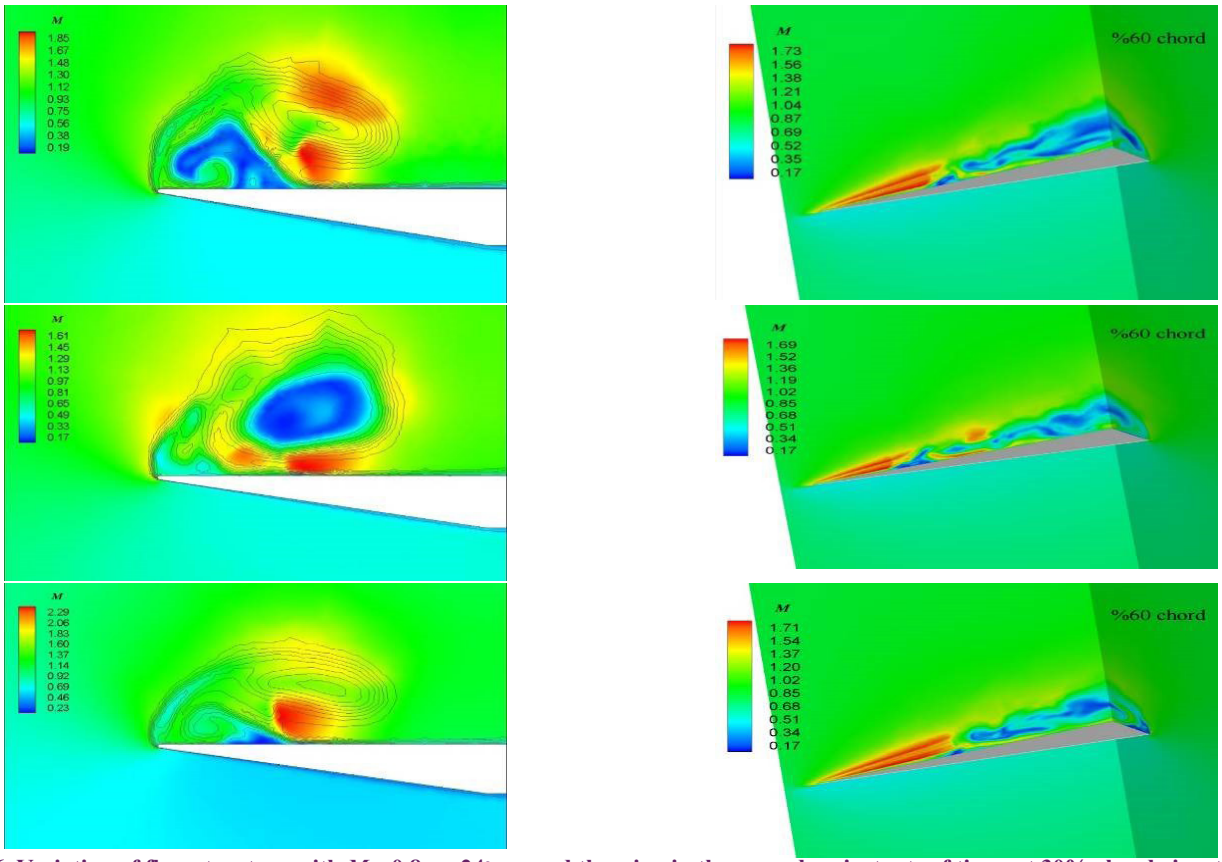

Fig. 6. Variation of flow structure with M_∞=0.8, α=24° around the wing in three random instants of time: at 30% chordwise station (left) and 60% chordwise station and a plane crossing the vortex axis (right)

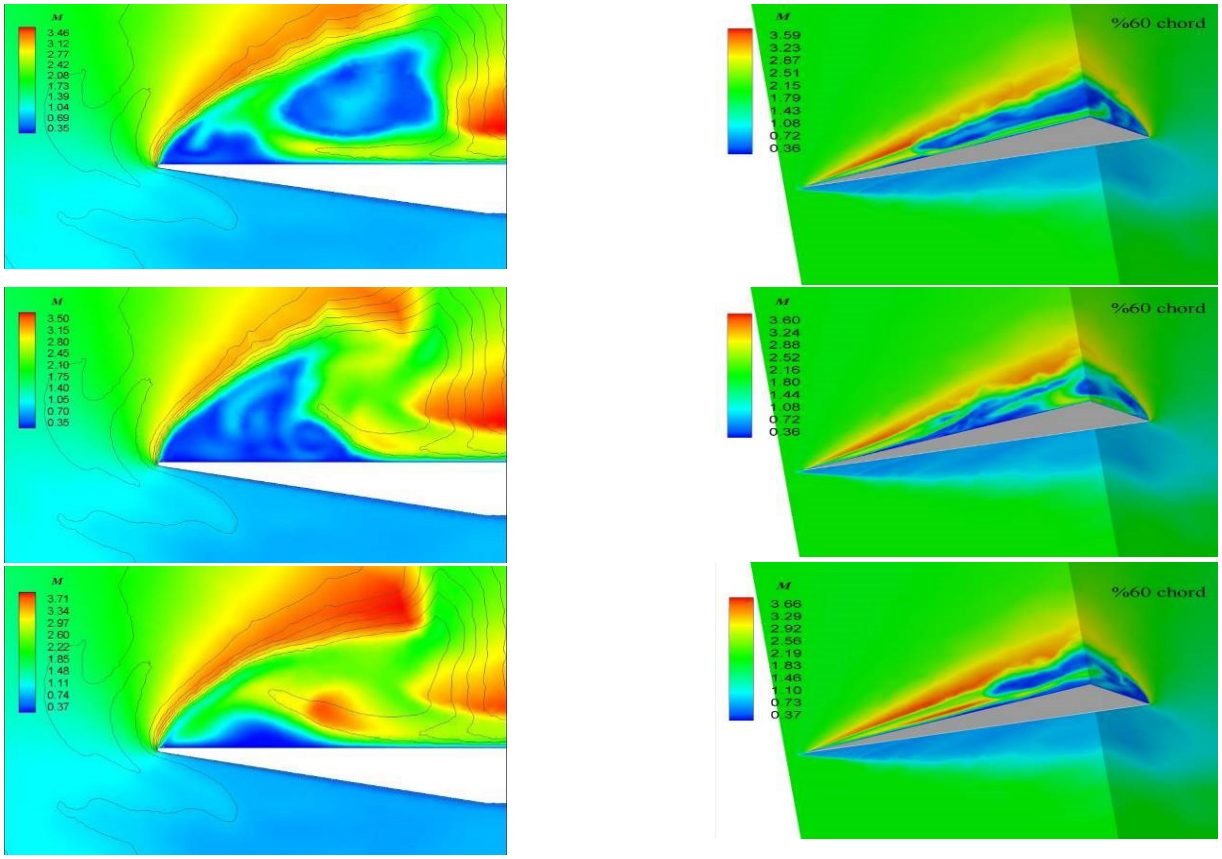

Fig. 7. Variation of flow structure with M_∞=2, α=44° around the wing in three random instants of time: at 30% chordwise station (left) and 60% chordwise station and a plane crossing the vortex axis (right)

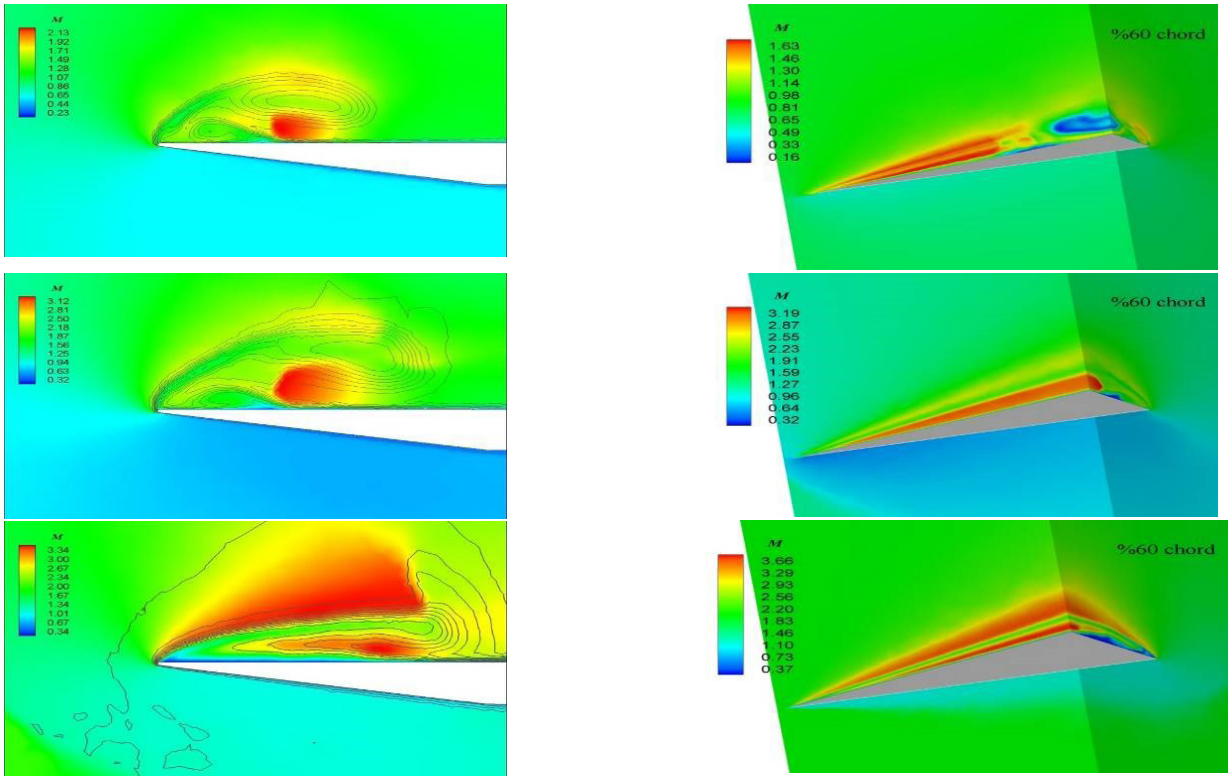

Fig. 8. Flow structure around the wing for different flow conditions at 30% chordwise station (left) and 60% chordwise station and a plane crossing the vortex axis (right)

Amongst the six flow conditions shown in Table 3, flow structure variations for three cases were shown in Figs 5 to 7. Instantaneous flow patterns for the remaining cases are shown in Fig. 8. The crossflow pattern for M_∞=0.8, α=20° is classical vortex with a crossflow shockwave below the primary vortex. For M_∞=1.2, α=30° the flow structure is vortex with a shock in which a weak oblique shock is seen above the primary vortex and a strong crossflow shock is seen below it. For M_∞=2, α=30° the flow structure is a separation bubble with a shock. A separation bubble is defined as a vortex without secondary separation. These patterns experience no significant changes with time. Only the random changes in the structure of breakdown region are observed for M_∞=0.8, α=20°. Obvious variations in flow pattern are seen when the free-stream Mach number is low enough and the angle of attack is high enough. The model geometry and Reynolds number in the present work are similar to those of Miller and Wood's experiments [8]. Therefore, a comparison between the numerical and experimental flow patterns can be made. Fig. 9 shows the comparison of a number of time-averaged numerical results with experimental flow visualization images of Miller and Wood obtained by the vapor screen technique. A good agreement is seen for all the flow conditions based on the vortical flow structures and the vortex-shock patterns. Some minor differences could be expected because the crossflow sections at which the patterns are shown are different. Also, the numerical patterns are time-averaged while the experimental patterns are instantaneous and could vary with time.

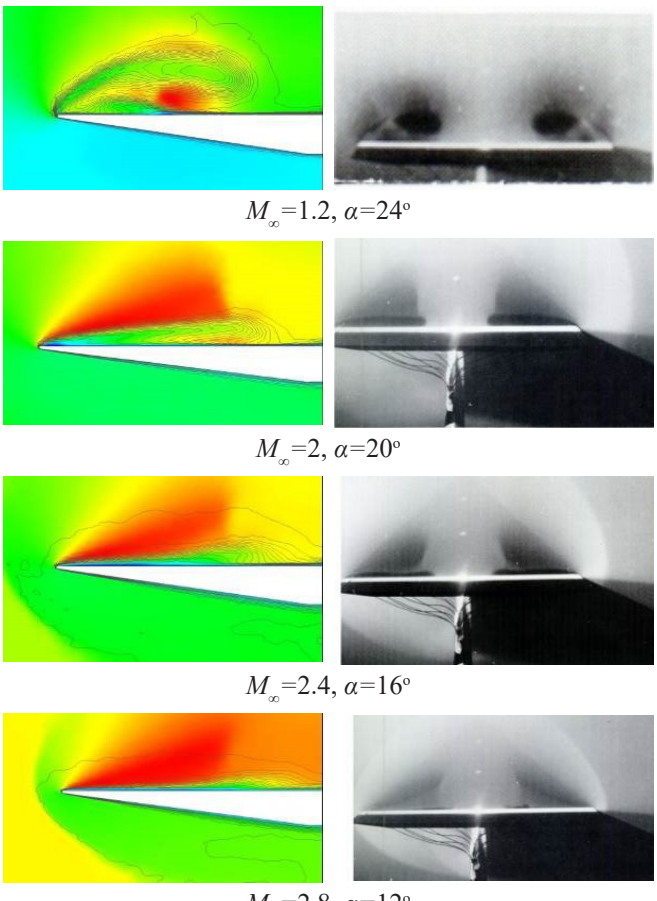

M_∞=1.2, α=24°

M_∞=2, α=20°

M_∞=2.4, α=16°

M_∞=2.8, α=12°

Fig. 9. Comparison of numerical time-averaged flow patterns with experimental flow visualization images of Miller and Wood[8]

3- 2- Unsteady Behaviour of Solution Parameters

To study the unsteady behaviour of the flow field in more detail, a number of point probes were situated in the computational domain. In each case, two probes were placed in the plane of 30% chordwise station, one near the primary vortex core and one in the vortex sheet. Some probes were also placed close to or downstream of breakdown location. Variations of u velocity component and static pressure coefficient with time at the probes were extracted from the unsteady solution. These data are used for the frequency analysis of the flow.

Fig. 10 shows an instantaneous picture of flow structure over the leeside of the wing at M_∞=0.4, α=20°. This figure shows an isosurface of vorticity magnitude with the coloring based on Mach number, the point probes (p1...p4), and the contours of vorticity magnitude in 30%, 60%, and 90% chordwise stations. The breakdown of vortex structure after the 30% chord section is obvious. The magnitude of vorticity is large in the regions of primary vortex core and shear layer separation from the leading edge, but it is substantially reduced after vortex breaks down. The coordinates (x/c , y/c , z/c) of the probes in this case are (0.300,0.050,0.090), (0.300,0.063,0.137), (0.730,0.090,0.220) and (0.920,0.087,0.287).

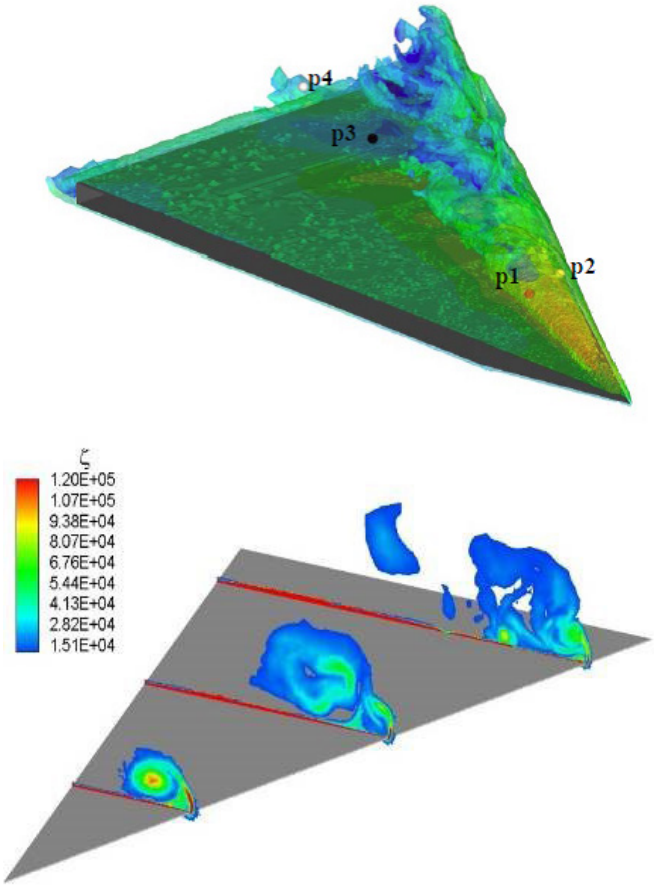

Fig. 10. Flow structure with M_∞=0.4, α=20°: an isosurface of vorticity with Mach contour and the selected probes (upper) and contour of vorticity at 30%, 60% and 90% chordwise stations (lower)

For M_∞=0.4, α=20°, Fig. 11 shows the plots of time history and power spectral density (PSD) versus frequency for non-dimensional u velocity component and C_p at the point probes.

The non-dimensional time is defined as $t^*=tU_\infty/c$ where t is the actual flow time. Points 1 and 2 are placed at the 30% chord plane where point 1 is closer to the vortex core. Points 3 and 4 are placed in the breakdown region where point 3 is closer to the breakdown mean location. At points 3 and 4, the time history exhibits a relatively large amplitude periodic oscillation. At points 1 and 2, the oscillation amplitude decreases significantly and the mean velocity is larger close to the vortex core. It is evident from the sudden drops in time history that the flow of these points does the reverse and therefore breakdown crosses the probes locations. At points 3 and 4 it approximately has the same values. Considering the frequency content of the signals given by the PSD plots, a number of dominant frequencies at each of the probe locations are obvious. In the following analysis, we consider the dominant frequencies for u PSD plots. The dominant frequencies of C_p PSD plots are almost similar. The most dominant frequencies found in points 1 and 2 occur at a non-dimensional frequency range of St=0.01-1.4 . The most dominant St values are 0.06 and 0.29 for points 1 and 2, respectively. Another dominant frequency for these two points occurs at St=7.3 with less amount of energy. A range of dominant frequencies found in points 3 and 4 occur at St=0.01-0.9 in which the most dominant values are 0.36 and 0.88 for points 3 and 4, respectively. The frequency St=0.06 is also present in this dominant range. As vortex breakdown has been shown to oscillate across this probe location, it is likely that these low frequencies are caused by the oscillation of the vortex breakdown location in the flow which also affects the upstream probes (points 1 and 2). Other dominant frequencies for points 3 and 4 are seen at St=1-5 with less energy content. These frequencies can be associated with the helical mode instability. For points 1 and 2, it is suggested that the dominant frequency St=7.3 is due to shear layer instabilities, such as the Kelvin-Helmholtz instability. Closer to the vortex core, the energy in this frequency content is lower.

Fig. 12 shows an instantaneous picture of flow structure over the leeside of the wing at M_∞=0.8, α=20°. This figure shows an isosurface of vorticity magnitude with the coloring

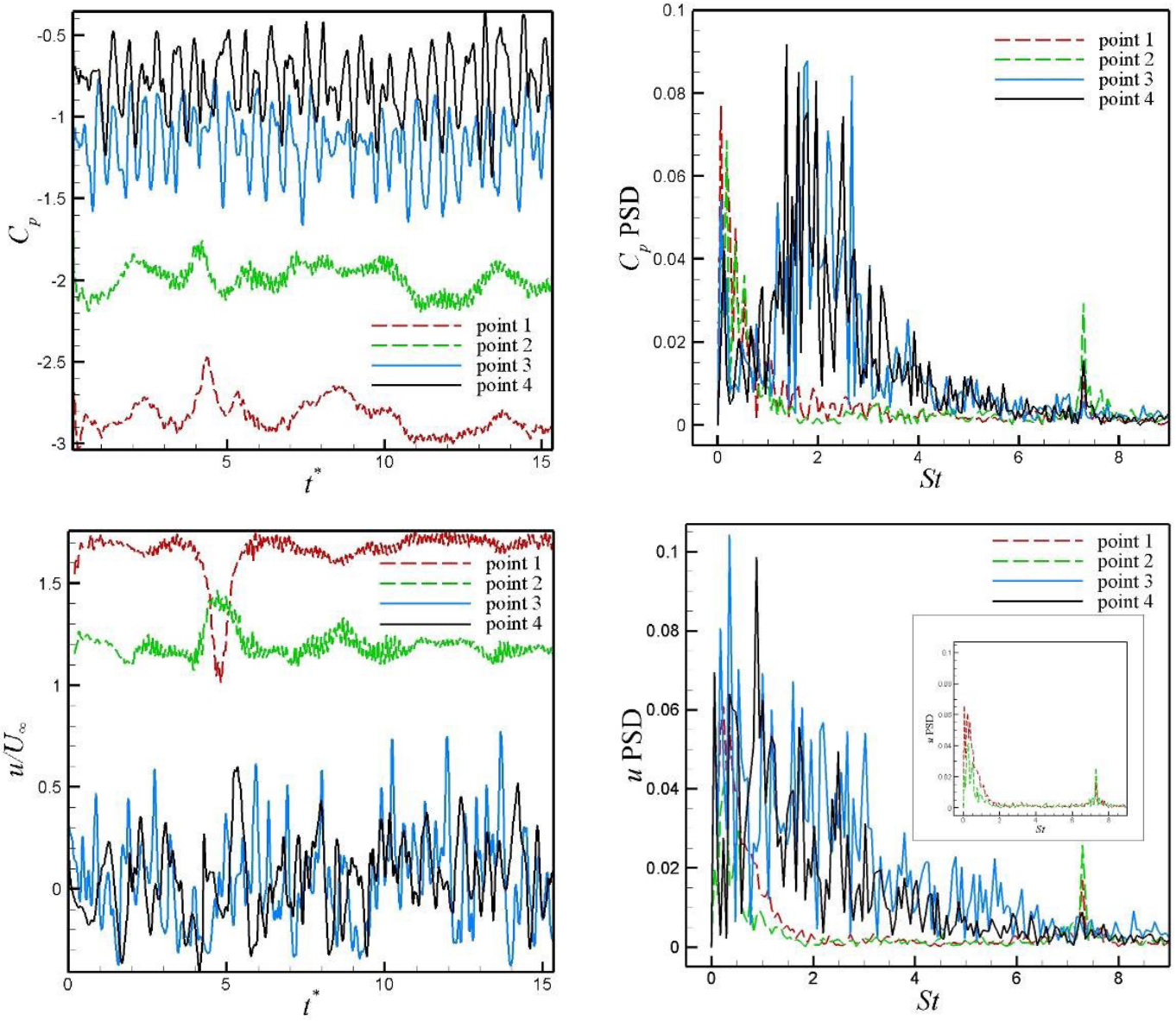

Fig. 11. Time history and PSD analysis of non-dimensional u velocity and C_p for M_∞=0.4, α=20°

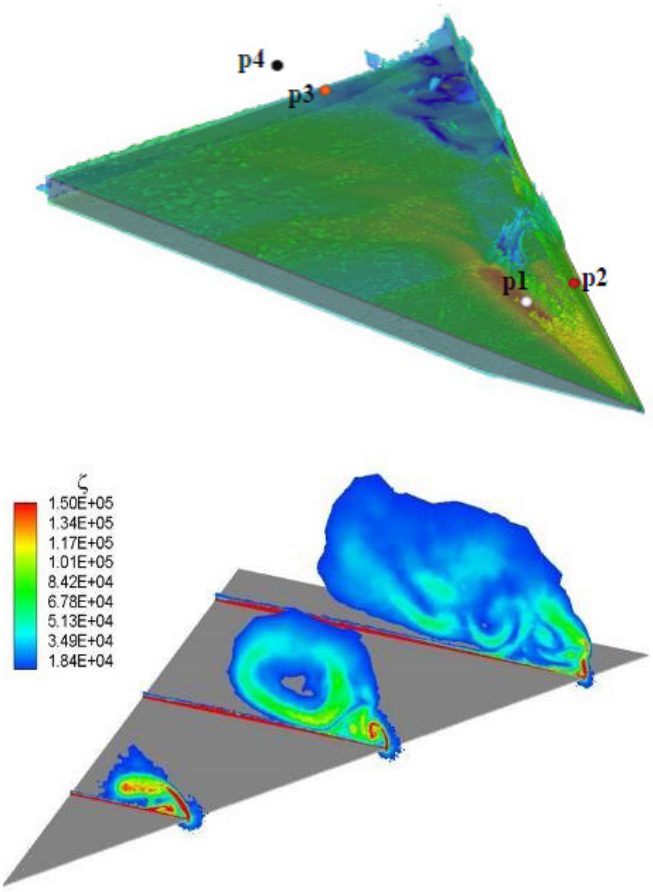

Fig. 12. Flow structure with M_∞=0.8, α=20°: an isosurface of vorticity with Mach contour and the selected probes (upper) and contour of vorticity at 30%, 60% and 90% chordwise stations (lower)

based on Mach number, the point probes (p1...p4), and the contours of vorticity magnitude in 30%, 60%, and 90% chordwise stations. The vorticity magnitude is large in the primary vortex core, secondary separation region, and the shear layer separated from the leading edge. Increasing Mach number makes adverse pressure gradient in the chordwise direction smaller and the location of breakdown moves downstream. Therefore, the primary vortex breaks down further downstream relative to the M_∞=0.4, α=20° case. The coordinates (x/c , y/c , z/c) of the probes in this case are (0.300,0.047,0.077), (0.300,0.050,0.143), (0.833,0.103,0.250) and (0.957,0.087,0.287).

For M_∞=0.8, α=20°, Fig. 13 shows the plots of time history and PSD versus frequency for non-dimensional u velocity component at the point probes. Points 1 and 2 are placed at the 30% chord plane where point 1 is closer to the vortex core. Points 3 and 4 are placed in the breakdown region where point 3 is closer to the breakdown mean location. At points 3 and 4, the time history exhibits a large amplitude periodic oscillation with a high frequency. The oscillations have larger amplitudes at point 3. At points 1 and 2, the signal becomes relatively constant and oscillation amplitude is very small. Mean u velocity magnitude is larger close to the vortex core. It has approximately the same value at points 3 and 4. It is evident that the flow of these points does the reverse and therefore breakdown crosses the probes locations. Considering the frequency content of the signals, the most dominant frequencies found in points 1 and 2 occur at a non-dimensional frequency range of St=0.01-0.5. The most dominant St value is 0.37 for both points. The most dominant range of frequencies found in points 3 and 4 occurs at St=0.01-0.9. The frequency St=0.37 is also present in this dominant range. As vortex breakdown has been shown to oscillate across this probe location, it is likely that these low frequencies are caused by the oscillation of the vortex breakdown location in the flow which also affects the upstream probes. Another dominant St range for points 3 and 4 is seen at St=1-2.5 which has more energy content at point 3 and the most dominant value of 1.33. It can be associated with helical mode instability. For points 1 and 2, a dominant frequency associated with shear layer instabilities is not detectable.

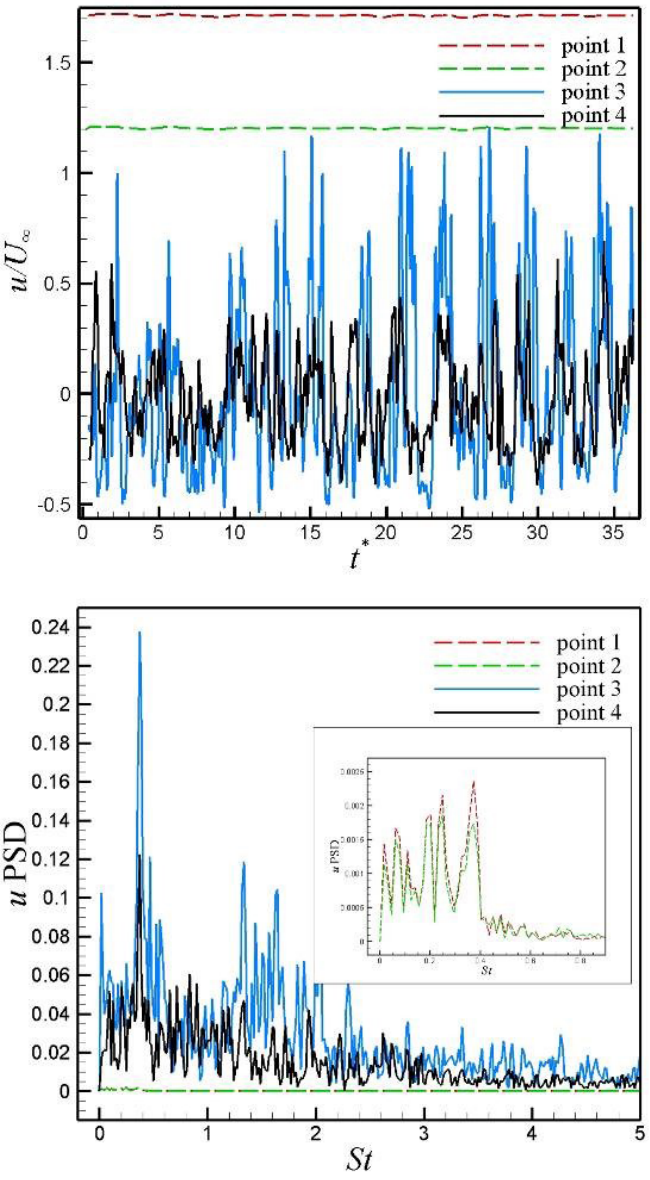

Fig. 13. Time history and PSD analysis of non-dimensional u velocity for M_∞=0.8, α=20°

Fig. 14 shows an instantaneous picture of flow structure over the leeside of the wing at M_∞=0.8, α=24° . This figure displays an isosurface of vorticity magnitude with the

coloring based on Mach number, the point probes (p1... p4), and the contours of vorticity magnitude in 30%, 60%, and 90% chordwise stations. Increasing the angle of attack causes the breakdown to move upstream. Therefore, the primary vortex breaks down further upstream relative to the M_∞=0.8, α=20° case. In fact, the breakdown location oscillates near the 30% chordwise station as depicted in Fig. 6. The coordinates (x/c , y/c , z/c) of the probes in this case are (0.300,0.053,0.073), (0.300,0.063,0.137), (0.720,0.090,0.217) and (0.853,0.080,0.257).

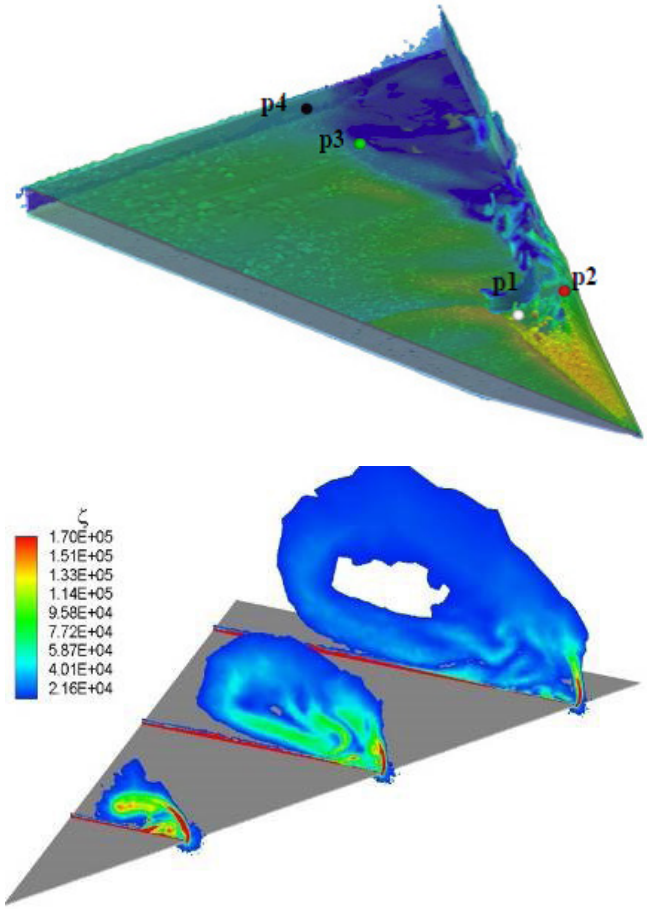

Fig. 14. Flow structure with M_∞=0.8, α=24°: an isosurface of vorticity with Mach contour and the selected probes (upper) and contour of vorticity at 30%, 60% and 90% chordwise stations (lower)

For M_∞=0.8, α=24°, Fig. 15 shows the plots of time history and PSD versus frequency of non-dimensional u velocity component at the point probes. Points 1 and 2 are placed at the 30% chord plane where point 1 is closer to the vortex core. Points 3 and 4 are placed in the breakdown region where point 3 is closer to the breakdown mean location. In this case, the breakdown location crosses the 30% chord plane; hence, the time history exhibits a large amplitude periodic oscillation at all points. The oscillations have larger amplitudes at point 1. Considering the frequency content of the signals, the most dominant frequencies found in the point 1 occur at a non-dimensional frequency range of St=0.01-2.6. The most dominant St values are 0.06 and 0.28 at this point. Similar values are observed for point 2 with a lower level of energy. It is likely that these low frequencies are caused by the oscillation of the vortex breakdown location in the flow. Some energy content is also seen at higher frequencies which can be related to the smaller structures existing in the flow. The most dominant range of frequencies found in points 3 and 4 occur at St=0.01-1.5 which can be associated with the oscillation of vortex breakdown location. Some energy content is seen at St=2-4 which can be associated with helical mode instability.

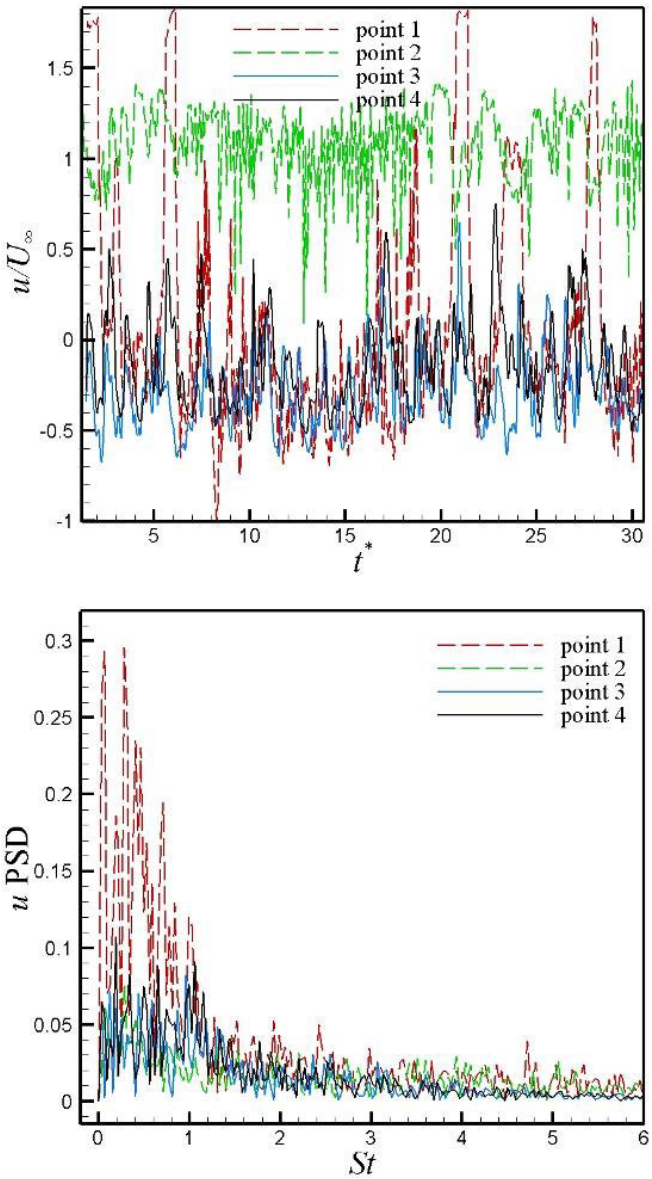

Fig. 15. Time history and PSD analysis of non-dimensional u velocity for M_∞=0.8, α=24°

Fig. 16 shows an instantaneous picture of flow structure over the leeside of the wing at M_∞=1.2, α=30°.This figure shows the isosurface of vorticity magnitude with the coloring based on Mach number, the point probes (p1...p3), and the contours of vorticity magnitude in 30%, 60%, and 90% chordwise stations. The primary vortex does not break down over the wing surface. However, the onset of breakdown starts in the secondary separation region from approximately half chord of the wing and expands to the whole vortex structure downstream of the wing. This causes the Mach

number and vorticity magnitude to decrease near the wing surface. The coordinates (x/c , y/c , z/c) of the probes in this case are (0.300,0.060,0.060), (0.300,0.070,0.107), and (1.037,0.060,0.413).

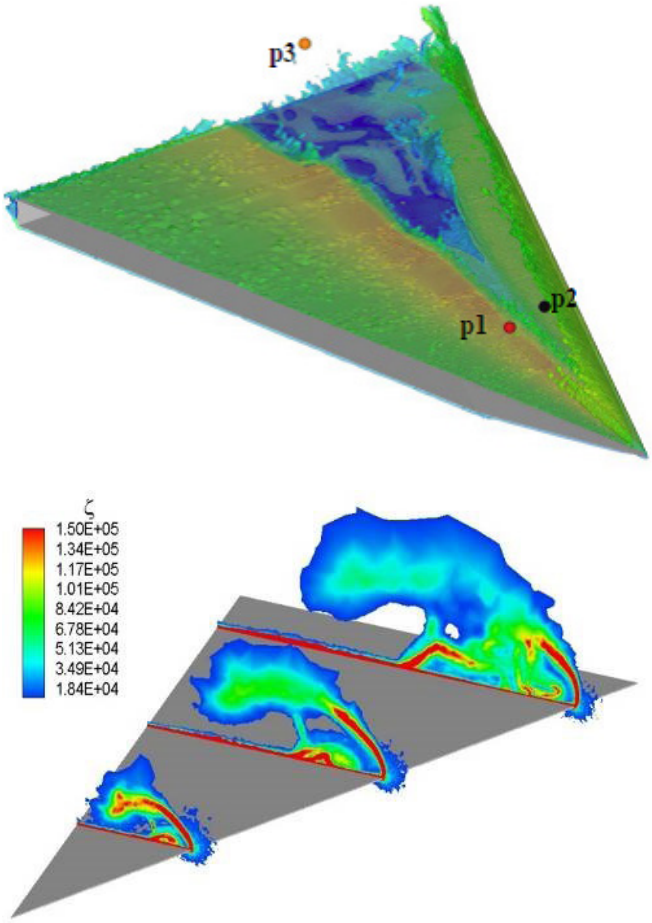

Fig. 16. Flow structure with M_∞=1.2, α=30°: an isosurface of vorticity with Mach contour and the selected probes (upper) and contour of vorticity at 30%, 60% and 90% chordwise stations (lower)

For M_∞=1.2, α=30°, Fig. 17 shows the plots of time history and PSD versus frequency of non-dimensional u velocity component at the point probes. Points 1 and 2 are placed at the 30% chord plane where point 1 is closer to the vortex core. Point 3 is placed in the breakdown region. At points 3, the time history exhibits a quasi-periodic oscillation with a positive mean value. At points 1 and 2, the signal becomes constant and oscillation is not observed. Mean u velocity is larger close to the vortex core. The most dominant range of frequencies found in points 3 occurs at St=0.01-0.85 as shown in the picture. The most dominant St value is 0.81. This range of dominant frequencies is probably caused by the oscillation of the vortex breakdown location.

Fig. 18 shows an instantaneous picture of flow structure over the leeside of the wing at M_∞=2, α=44°. This figure displays the isosurface of vorticity magnitude with coloring based on Mach number, the point probes (p1...p4), and the contours of vorticity magnitude in 30%, 60%, and 90% chordwise stations. Increasing the angle of attack causes the breakdown to occur even at the supersonic regime. In this case, the breakdown location oscillates near the 30% chordwise station as depicted in Fig. 6. The vorticity magnitude in the shear layer is large even after vortex breakdown. The coordinates (x/c , y/c , z/c) of the probes in this case are (0.300,0.070,0.033), (0.300,0.067,0.077), (0.767,0.107,0.153) and (0.923,0.083,0.187).

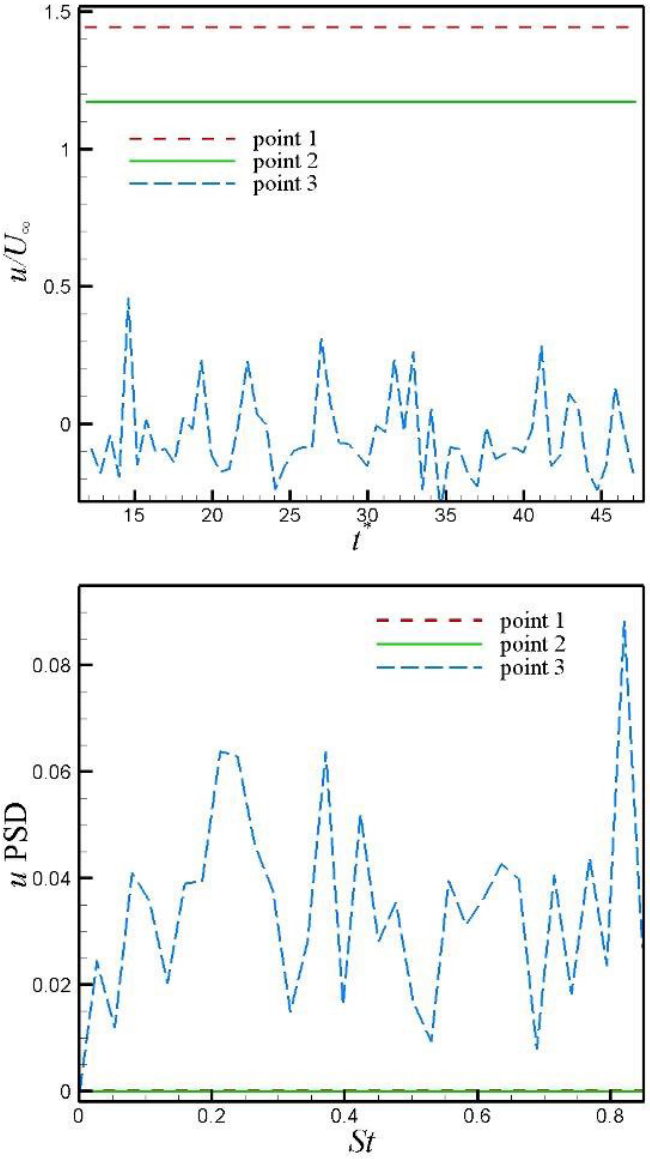

Fig. 17. Time history and PSD analysis of non-dimensional u velocity for M_∞=1.2, α=30°

For M_∞=2, α=44°, Fig. 19 shows the plots of time history and PSD versus frequency of non-dimensional u velocity component at the point probes. Points 1 and 2 are placed at the 30% chord plane where point 1 is closer to the vortex core. Points 3 and 4 are placed in the breakdown region where point 3 is closer to the breakdown mean location. The breakdown location crosses the 30% chord plane; hence the time history exhibits a large amplitude periodic oscillation at the probes in this plane, especially the point 2. Sudden drops in u velocity magnitude of point 2 imply the pass of vortex breakdown location through this point. The fluctuations of breakdown location seem to be more pronounced for this case; however, this is likely to be due to the presence of shock waves in the

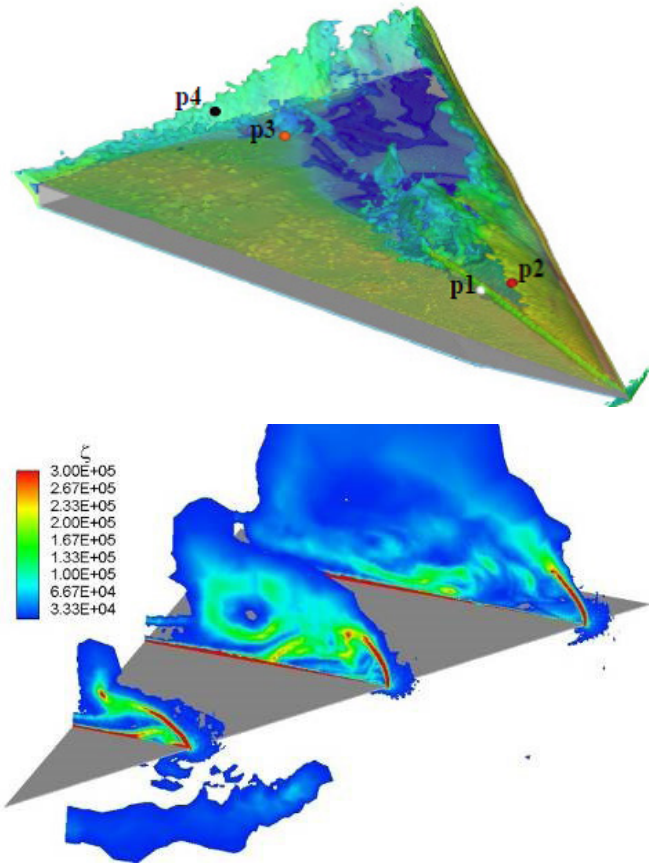

Fig. 18. Flow structure with M_∞=2, α=44°: an isosurface of vorticity with Mach contour and the selected probes (upper) and contour of vorticity at 30%, 60% and 90% chordwise stations (lower)

flow, which have been found to move abruptly. It is also clear that there is less unsteadiness in the flow when the breakdown location is upstream of the probe. An approximately similar range of dominant frequencies (St=0.01-1.5) is seen for all probes. St=0.06 is the most dominant for points 1 and 2 which exhibits considerably a high amount of energy at point 2 and can be related to the vortex breakdown oscillation.

From the analyses performed for different flow conditions, it was shown that low frequencies associated with vortex breakdown oscillation are the most dominant frequencies in all cases where vortex breakdown occurs. Dominant frequencies associated with helical mode instability are also present at the probes downstream of breakdown. Dominant frequencies related to the shear layer instabilities were distinctly observed only for the low subsonic regime. These results are quite in agreement with those reported by Schiavetta et al. [4]. They did similar studies for a 70° delta wing at M_∞=0.2, α=27° and a 65° delta wing at M_∞=0.85, α=23°. Also, the numerical values of the frequency ranges obtained in the present work agree well with the values shown in Table 1.

Fig. 20 shows the time history of lift coefficient for the flow conditions discussed above. The mean lift coefficient for each case is also written in the figure. The magnitude of mean lift coefficient increases with the increase of Mach number at a fixed angle of attack in subsonic regime and decreases with the increase of Mach number at the supersonic regime. By increasing the angle of attack, the mean lift increases. For subsonic conditions, most of the wing leeside is in the

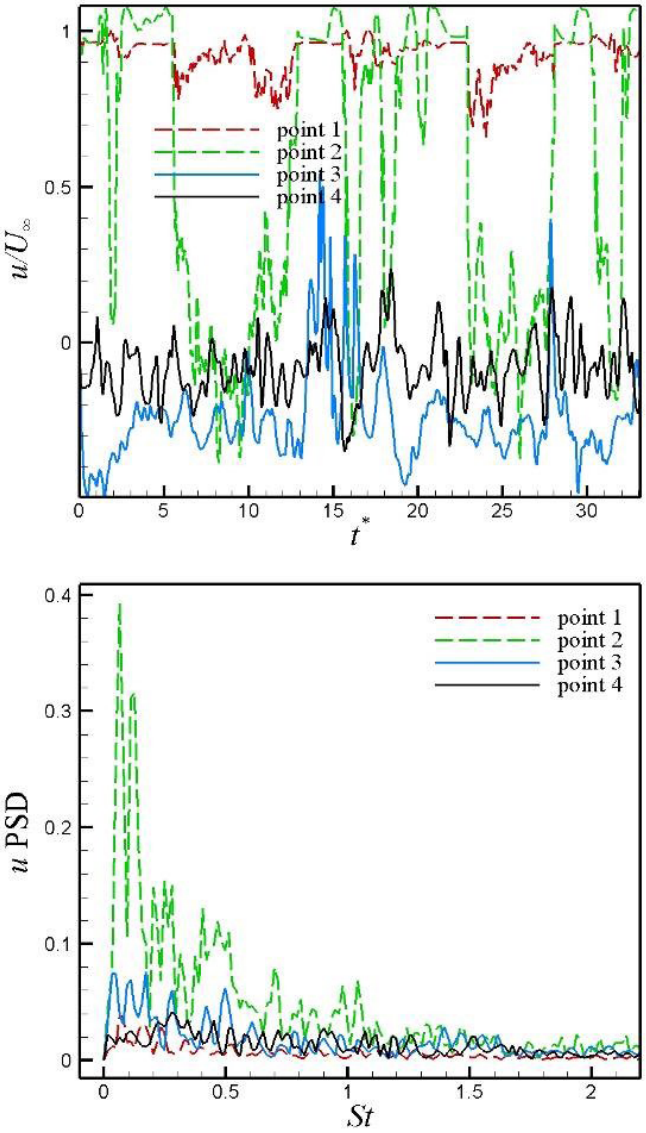

Fig. 19. Time history and PSD analysis of non-dimensional u velocity for M_∞=2, α=44°

breakdown region which makes the mean lift coefficient to be reduced. Only for subsonic conditions is seen a considerable oscillation in lift coefficient with respect to the time. The lift coefficient in supersonic conditions exhibits an approximately constant value, even for the conditions where vortex breakdown occurs. Variation in lift coefficient with time is mostly dependent on the oscillations in vortex breakdown location. It can be concluded that despite the existence of dominant frequencies in supersonic conditions associated with vortex breakdown oscillation, its amplitude is not so large that it could affect the lift coefficient considerably.

4- Conclusions

A DES solver was used to simulate the unsteady vortical flow structures over a 60° delta wing at various Mach numbers and moderate angles of the attack. From the analysis of the solutions, it is clear that there are a number of dominant flow features, which occur in the flow over a delta wing. The main features found are associated with the motion of vortex breakdown location, the helical mode instability of vortex breakdown, and possible shear layer instabilities.

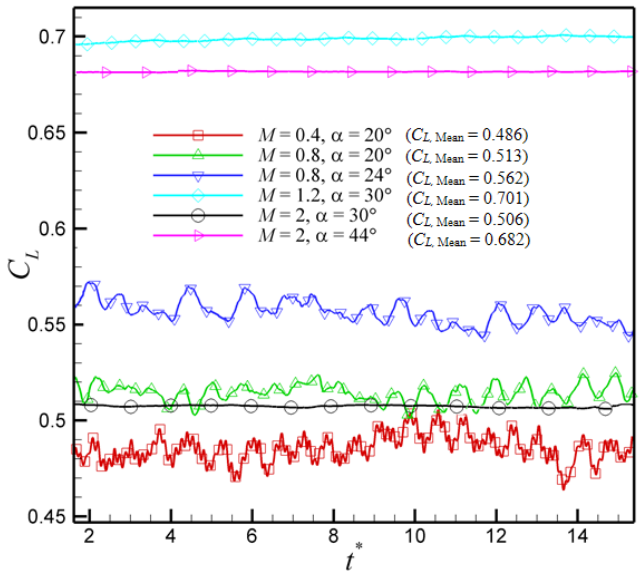

Fig. 20. Time history of the lift coefficient for different flow conditions

Each phenomenon makes different frequencies to be dominant at different positions in the flow field. Through the frequency analysis of the *u* velocity at the probes located in the flow field, it was shown that low frequencies associated with vortex breakdown oscillation are the most dominant frequencies in all cases where vortex breakdown occurs. Dominant frequencies associated with helical mode instability are also present at the probes downstream of breakdown. Dominant frequencies relevant to the shear layer instabilities were distinctly observed only for the low subsonic regime. The structures which occur appear to be periodic in nature. Upstream of breakdown, the type of crossflow pattern does not change with time, except for minor changes in local variables distributions in low Mach number conditions. Downstream of breakdown, the flow structure varies with time. A quasi-periodic behaviour was observed for lift coefficient in subsonic cases. The lift coefficient in supersonic conditions exhibited an approximately constant value, even for cases where vortex breakdown occurs.

References

[1] I. Gursul, Recent Developments in Delta Wing Aerodynamics, *Aeronautical Journal*, 108(1087) (2004) 437-452.

[2] I. Gursul, Reviews of Unsteady Vortex Flows over Slender Delta Wings, *Journal of Aircraft*, 42(2) (2005) 299-319.

[3] R.C. Nelson, A. Pelletier, The Unsteady Aerodynamics of Slender Wings and Aircraft Undergoing Large Amplitude Maneuvers, *Progress in Aerospace Sciences*, 39 (2003) 185-248.

[4] L.A. Schiavetta, K.J. Badcock, R.M. Cummings, Comparison of DES and URANS for Unsteady Vortical Flows over Delta wings, in: *45th AIAA aerospace science and meeting exhibit*, Reno, Nevada, USA, 2007.

[5] P.R. Spalart, W.H. Jou, M. Strelets, S.R. Allmaras, Comments on the Feasibility of LES for Wings and on a Hybrid RANS/LES Approach, in: Advances in DNS/LES, *1st AFSOR international conference on DN/LES, AFSOR*, 1997.

[6] A.M. Mitchell, S.A. Morton, J.R. Forsythe, R.M. Cummings, Analysis of Delta Wing Vortical Substructures Using Detached Eddy Simulation, *AIAA Journal*, 44(5) (2006) 964-972.

[7] S.A. Morton, High Reynolds Number DES Simulations of Vortex Breakdown over a 70º Delta Wing, in: *21st applied aerodynamic conference*, 2003.

[8] D.S. Miller, R.M. Wood, Leeside Flows over Delta Wings at Supersonic Speeds, *Journal of Aircraft*, 21(9) (1984) 680-686.

[9] S.N. Seshadri, K.Y. Narayan, Possible Types of Flow on Lee-Surface of Delta Wings at Supersonic Speeds, *Aeronautical Journal*, 92(915) (1988) 185-199.

[10] M.D. Brodetsky, E. Krause, S.B. Nikiforov, A.A. Pavlov, A.M. Kharitonov, A.M. Shevchenko, Evolution of Vortex Structures on Leeward Side of a Delta Wing, *Journal of Applied Mechanics and Technical Physics*, 42(2) (2001) 243-254.

[11] M. Hadidoolabi, H. Ansarian, Computational Investigation of the Flow Structure over a Pitching Delta Wing at Supersonic Speeds, Proceedings of the Institution of Mechanical Engineers, Part G: *Journal of Aerospace Engineering*, 230(7) (2015) 1334-1347.

[12] M. Hadidoolabi, H. Ansarian, Computational Investigation of Vortex Breakdown over a Pitching Delta Wing at Supersonic Speeds, *Scientia Iranica* (B), In Press (2017).

[13] P.R. Spalart, S.R. Allmaras, A One Equation Turbulence Model for Aerodynamic Flows, in: *30th AIAA aerospace science and meeting exhibit*, USA, 1992.

[14] J.R. Forsythe, K.A. Hoffmann, F.F. Dieteker, Detached-Eddy Simulation of a Supersonic Axisymmetric Base Flow with an Unstructured Flow Solver, *AIAA Paper*, (2000).

Please cite this article using:

H. Ansarian and M. Hadidoolabi, Computational Investigation of Unsteady Compressible Flow over a Fixed Delta Wing Using DES, *AUT J. Mech. Eng.*, 1(2) (2017) 219-232.

DOI: 10.22060/mej.2017.12863.5455